ARTICLE

Received 00th January 20xx,

Accepted 00th January 20xx

DOI: 10.1039/x0xx00000x

Investigation of Transcription Factor-DNA Binding with Electrolyte-Gated Organic Transistors

Matteo Sensi,[a]* Andrea Ricci,[a] Giovanna Rigillo,[a] Alessandro Paradisi,[a] Marcello Berto,[a] Nerina Gnesutta,[b] Carol Imbriano,[a] Fabio Biscarini,[a,c] and Carlo Augusto Bortolotti [a]

Nuclear transcription Factor Y (NF-Y) is a CCAAT-binding trimeric protein. The overexpression of the DNA binding subunit A (NF-YA) results in a deregulation of many CCAAT-dependent pro-growth genes in multiple tumor types. Exon 3 alternative splicing of NF-YA results in two different isoforms, NF-YAs (short) and NF-YAl (long), which can promote tumor proliferation or metastasis, respectively. In this work, we developed an electrolyte-gated organic transistor (EGOT) biosensor to study the binding of NF-YAl-composed NF-Y complex to its consensus sequence. We show that by using the target DNA sequence as probe, the device detects NF-Y in a range between 1 pM to 10 nM. Control experiments performed with oligonucleotides probes mutated in the consensus sequence exhibit weaker, though not fully hindered, binding to NF-Y compared to the response to unmutated DNA. This behavior confirms that also the base pairs near the CCAAT-box have a role in the transcription factor recognition. Furthermore, we contributed to the advance of the present state of the art by demonstrating the ability of the EGOT biosensor to detect NF-Y in cell lysate, a fundamental step towards the development of point-of-care (POC) devices for the analysis of biopsies.

Introduction

Transcription factors (TFs) are proteins which control gene expression by binding specific DNA recognition sequences, called consensus sequences, allowing cells to respond to both internal and external stimuli. By ensuring the correct expression of specific genes, the transcriptional regulatory system plays a central part in controlling many biological processes, ranging from cell cycle progression, maintenance of intracellular metabolic and physiological balance to cellular differentiation and developmental time courses.[1]

Nuclear Factor Y (NF-Y) is a transcription factor whose regulome and interactome are essential for healthy tissue homeostasis, cell survival and metabolic function.[2–6] Its crucial action can, on the other hand, become harmful when misregulated, being involved in transformation and/or progression of different types of cancer. [2,6–9]

NF-Y is a trimeric protein, composed by the subunits NF-YA, NF-YB and NF-YC. [10] NF-YA provides selective DNA binding at a specific motif, named CCAAT box, which is one of the most common promoter elements found in approximately one-third of eukaryotic housekeeping and lineage-specific genes.[11] Besides, the NF-Y binding site is frequently found in regulatory regions of cell proliferation, cell death and key metabolic genes.[4,12] In order to form the NF-Y/CCAAT complex, the NF-YA subunit must first associate with NF-YB/NF-YC to heterodimerize *via* their histone-fold domains (HFDs), forming a scaffold for NF-YA.

The NFYA gene encodes for two splice variants, NF-YAs (short) and NF-YAl (long), which differ by 28 amino acids. The two isoforms have been shown to affect activation of specific sets of genes:[12] while NF-YAs supports cell proliferation in stem and muscle cells, NF-YAl seems to induce differentiation.[4,13,14] In tumor cells, NF-YAs has been generally associated with poor differentiation and high proliferation and a general unbalance of the NF-YAl/NF-YAs ratio towards the short subunit characterizes solid cancers,[7,9,15,16] although with some exceptions. Oppositely, NF-YAl high levels correlate with the overexpression of pro-migration genes and drives epithelial to mesenchymal transition (EMT) in aggressive tumors.[4,7,9,17]

The detection and quantification of NF-YA isoforms in biopsies could improve the evaluation of the progression stage of cancers. In literature, some examples of biosensors for the detection of transcription factors are reported.[18-20] Nevertheless, all these biosensors are characterized by the need of expensive instrumentation and by the fact that their response is based on the presence of labels.

Electrolyte-Gated Organic Transistors (EGOTs) are an emerging technology in the field of label-free biosensing for healthcare, food and environmental applications, thanks to their

[a] Dipartimento di Scienze della Vita, Università degli Studi di Modena e Reggio Emilia, via Campi 103, Modena 41125, Italy. E-mail: matteo.sensi@unimore.it
[b] Dipartimento di Bioscienze, Università degli Studi di Milano, Via Celoria 26, Milano 20133, Italy.
[c] Center for Translational Neurophysiology, Istituto Italiano di Tecnologia, Via Fossato di Mortara 17–19, Ferrara 44121, Italy

outstanding performances in terms of limit of detection and selectivity.[21–27] In the literature are reported EGOT biosensors for the detection in test solutions of a wide range of clinically relevant diagnostic biomarkers for various diseases, infections, syndromes, and cancer conditions.[28–31] No biosensors based on EGOT architecture have been reported so far for the detection of transcription factors.

In this work, we report on the first label-free EGOT biosensor for the detection of the transcription factor NF-Y composed by the NF-YA long isoform. Moreover, aiming towards a long-term goal of applying this technology to liquid biopsies, we demonstrate that the EGOT biosensors can detect the target not only in buffer solutions but also in a complex biological sample such as cell lysate. This research could be a valid starting point for the realization of a powerful tool for both *in vitro* DNA-TF interaction studies and clinical analysis in tumor diagnostics and characterization, by detection and quantification of the two NF-YA isoforms.

Results and discussion

We fabricated a biosensor based on the Electrolyte-Gated Organic Transistor (EGOT) architecture, where two interdigitated source and drain electrodes (W/L= 49000, interdigitated Ø= 3.5 mm) are covered with a p-type organic semiconductor (TIPS-pentacene), deposited by drop-casting on gold interdigitated source and drain electrodes, on a glass substrate (Micrux©, Fig. 1), and cured in the oven at 60 °C for 30 minutes. A drop of 1X PBS buffer acting as dielectric layer was confined on the channel by a PDMS pool, connecting the semiconductor with the gold gate electrode (Ø=3 mm). The biorecognition event between NF-Y and the double-stranded oligonucleotides containing the consensus sequence takes place at the gate electrode, where we immobilized the target DNA probe. To obtain this result, the gold surface of the gate has been functionalized by the following steps: i) formation a 11-mercapto-undecanoic (MUA): 6-mercaptohexanol (MCH)

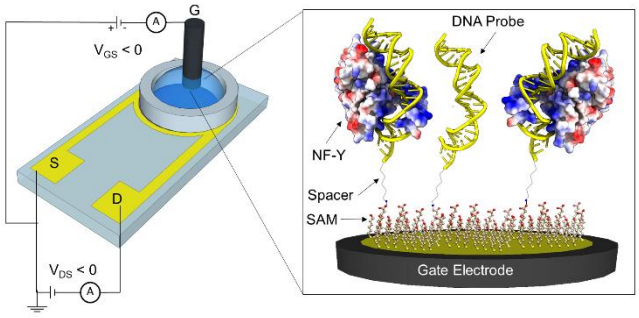

Fig. 1 Gate functionalization scheme. Scheme of the final device configuration and connection. The inset shows the magnification of the gate electrode covered with the SAM, where the dsDNA probe has been immobilized to achieve NF-Y detection. The structure of the NF-Y/DNA complex was taken from the Protein Data Bank (PDB code: 4AWL).

1:3 self-assembled monolayer (SAM);[32,33] ii) binding of a 26 base-pairs oligonucleotide, containing a C-6 space, the CCAAT box and a terminal amine, to the carboxylic groups of MUA by means of 1-Ethyl-3-(3-dimethylaminopropyl)carbodiimide/N-hydroxysuccinimide (EDC/NHS); iii) complementary oligonucleotide hybridization to obtain a dsDNA (Fig. 1 inset); iv) blocking of unreacted intermediates with 10 mM Tris, for 30 minutes.

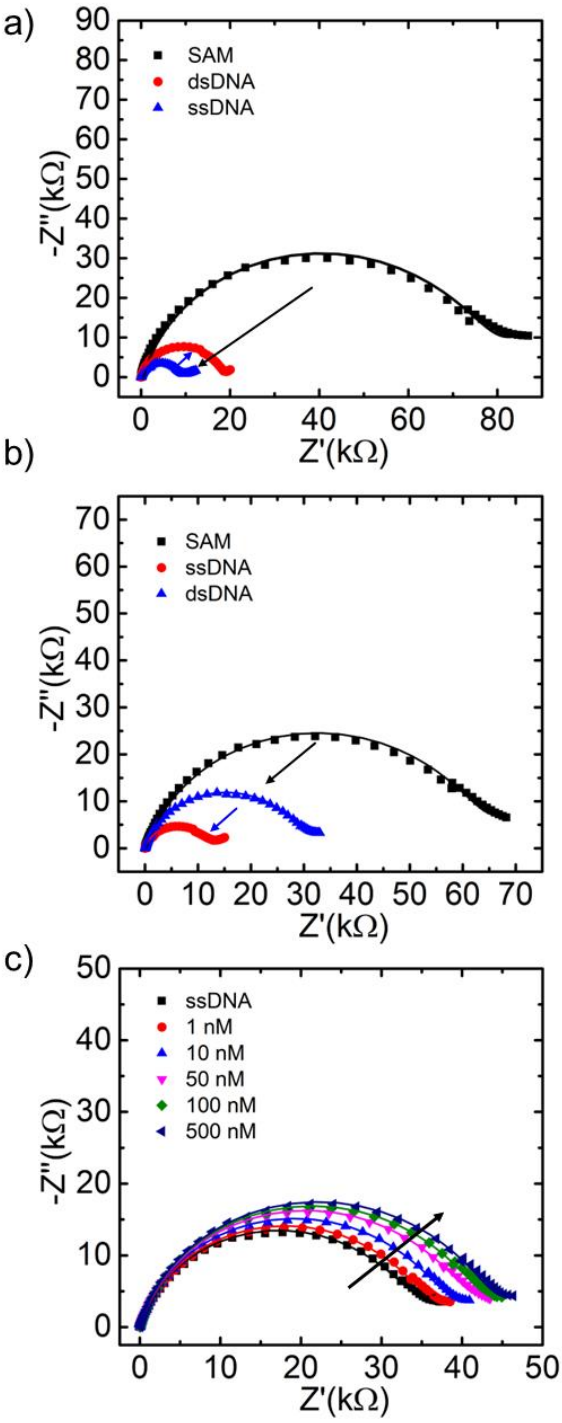

Fig. 2 Electrochemical characterization of the DNA probe immobilization. a) Nyquist plot showing the impedance of Au gate electrode covered with the mixed SAM. (MUA/MCH, black), the covalently bound oligonucleotide (ssDNA, blue) and the complementary strand (dsDNA, red). b) Melting of the complementary strand from the dsDNA, by heating at 80°C for 10 min after incubation in the dsDNA. c) Detection of increasing concentrations of the complementary oligonucleotide. All measurements were performed in 5 mM $K_3Fe(CN)_6$, 1 M KCl. The lines are the results of the fitting with a modified Randles circuit (see experimental section and Figure S2 for details).

We monitored the functionalization steps by faradic electrochemical impedance spectroscopy in presence of 5 mM $K_3[Fe(CN)_6]$ as redox probe. As shown in Fig. 2a, the high impedance induced by the presence of the SAM on the gate is reduced upon immobilization of the oligonucleotide, which is due to the conversion of the acid groups to amide bonds and to partial destabilization of the SAM induced by the EDC/NHS treatment, as previously observed in the literature.[34,35] By exposing the gate to 1 µM complementary oligonucleotide, we observe the formation of the dsDNA, which is characterized by an increase of impedance of ~2 times if compared to that of

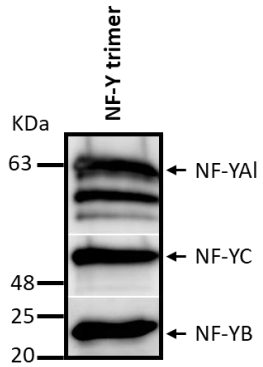

Fig. 3 NF-Y trimer assembly. Immunoblot analysis of the NF-Y trimer assembly composed by NF-YAl, NF-YB and NF-YC. The single subunits were detected with the appropriate antibody (anti-NF-YA, anti-NF-YB, anti-NF-YC).

ssDNA. To further investigate the immobilization of the DNA on the gate electrode surface,[36–38] we immobilized the dsDNA directly on the electrode after in solution hybridization between the probe and the complementary oligonucleotide. By heating at 80 °C for 10 minutes, and then collecting EIS spectra, we observed the melting of the dsDNA by halving of the impedance back to ssDNA values (Fig. 2b). Finally, as shown in Fig. 2c, we demonstrate the presence of the oligonucleotide single stranded probe bound on the electrode surface by performing the detection of the complementary strand at increasing concentrations, ranging from 1 nM to 500 nM.[39,40]

We observed an increase of the resistance to the electron transfer from ferricyanide to the gate electrode as the gate is exposed to increasing concentrations of the complementary strand, suggesting the formation of dsDNA on the gate and an increase of redox probe repulsion, due to the negative charge of the phosphate groups on the surface. We then produced the NF-Y trimer composed by NF-YAl, and the NF-YB/NF-YC subunits dimer. Purified recombinant proteins produced in E. coli from mouse cDNAs were incubated in 100 mM salt solution buffer for 2 h to allow the assembly of the NF-Y complex (Fig. 3).

The presence of DTT in the NF-Y complex-containing buffer could lead to the reduction of the S-Au bond which links the MUA/MCH self-assembled monolayer to the gate surface. To avoid this issue, we performed a buffer exchange using an AMICON Centrifugal Filter Unit with a 10 kDa cutoff, removing DTT by four successive centrifuge and recover steps. As shown

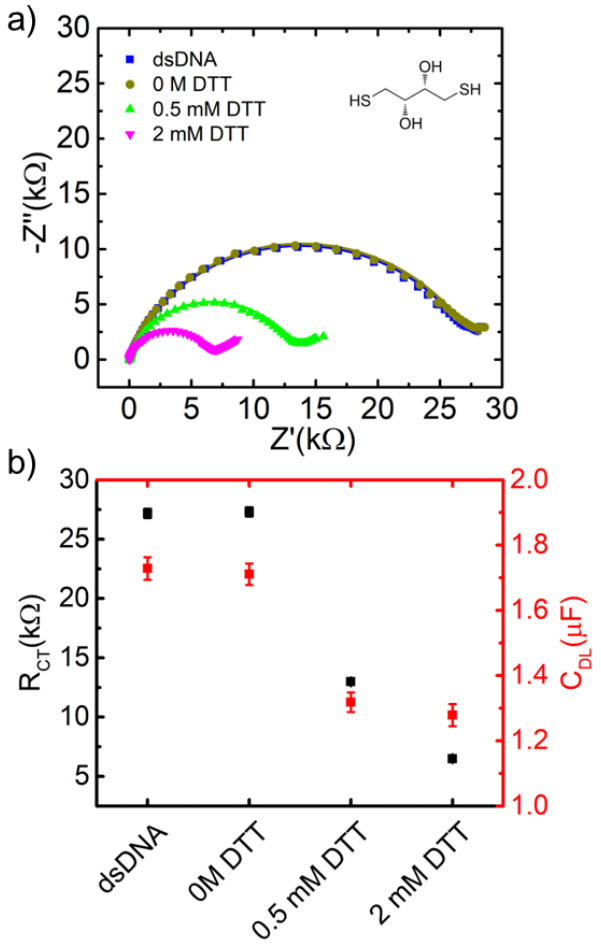

Fig. 4 DTT influence on the gate functionalization. a) Nyquist plots obtained from faradic EIS of the functionalized gate electrode exposed to increasing concentrations of DTT. The lines are the results of the fitting with a modified Randles circuit (see experimental section). b) Values of charge transfer resistance (R_{CT}) and double layer capacitance (C_{DL}) obtained from the fit, as a function of DTT.

in Fig. 4a, upon exposure of the fully functionalized gate (black squares) to the protein buffer containing DTT (0.5 mM and 2 mM), both imaginary and real parts of the impedance decrease, suggesting a detachment of the SAM by DTT or its replacement with DTT itself. By fitting the impedance curves with a modified Randles circuit, where we introduced a constant phase element instead of a capacitor, we extracted the resistance to charge transfer (R_{CT}) and the double layer capacitance (C_{DL}) upon each step. The results in Fig. 4b show that the incubation of the functionalized gate with the protein buffer without DTT has no effect on the functionalization stability; on the other hand, the exposure of the gate to 0.5 mM and 2 mM DTT decreases R_{CT} from 27 kΩ to 12.5 kΩ and then to 7.5 kΩ suggesting the detachment of the previously formed SAM from the gold surface.

We then used gold electrodes, functionalized with dsDNA containing the CCAAT box as described above, to gate an EGOT device to perform the detection of the transcription factor freely diffusing in solution, exploiting the direct binding of the

TF to the consensus CCAAT sequence of the oligonucleotide probe. To do so, we incubated the functionalized gate electrode in solutions of increasing concentrations of NF-Y in TRIS buffer for 15 minutes and then we recorded the transfer curves of the EGOT. NF-YA cellular concentration has not been yet determined, however, for most of the TF the concentrations are in the pM to nM range, for this reason we selected concentrations between 1 pM to 10 nM.[41,42] As shown in Fig. 5a, the drain-source current in the TIPS-Pentacene channel (I_{DS}) increases monotonically upon binding of NF-Y to the DNA probe until 10 nM, when a saturation of the response is observed. We estimated a limit of detection (LOD) of 10 fM (see experimental section for the definition).

NF-Y is a negatively charged protein at physiological pH (pI = 5.6); the increase of I_{DS} current upon binding of negatively charged species was previously observed[41–43] and can be reconducted to the change of effective gate-source voltage (V_{GS}), due to the presence of negatively charged species on the gate. Consequently, the channel reacts like if a more negative gate potential is applied and hence there is an increase of the charge carriers (holes) density, which in turn increases the current. Nevertheless, we are aware that the target charge cannot be the only determining factor to the magnitude and sign of the drain current shift upon binding, as the changes are strongly dependent also on the functionalization strategy, the chemical natura of the probe and features of the surface, which all contribute to the changes in the electrical double layers at the gate/electrolyte interface as well as to shifts of the electrochemical potential of the gate itself.

Recording the EGOT transfer curves allows to extract several characteristic parameters of the operating transistor, which can

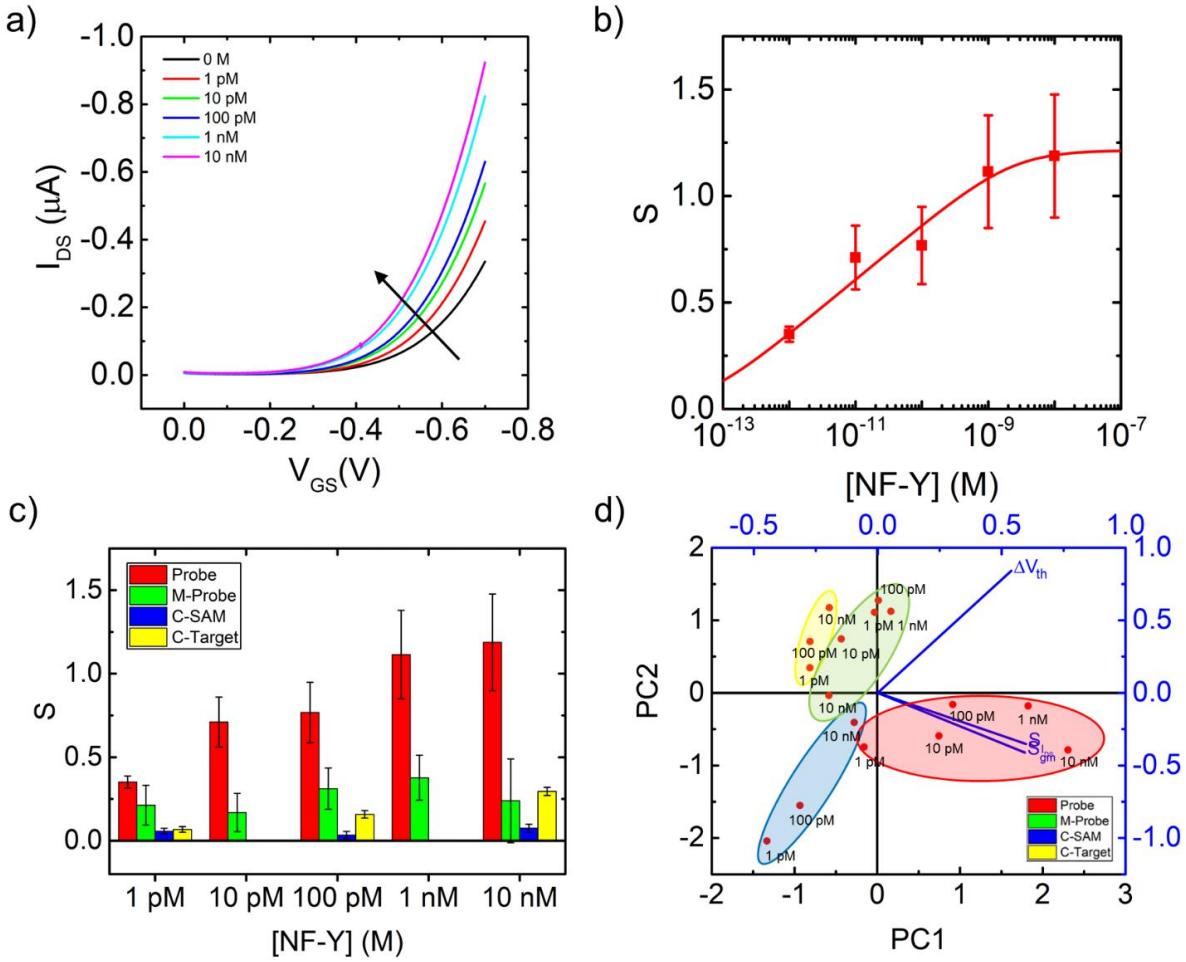

Fig. 5 NF-Y detection. a) Transfer curves of the EGOT biosensor with the gate incubated in increasing concentrations of NF-Y measured with a 1X PBS drop on the device applying a fixed V_{DS} = -0.2 V. b) Dose curve for NF-Y with the consensus DNA sequence (Probe) on the gate electrode at V_{GS} = -0.5 V. The data are fitted with a uniform Langmuir absorption model. c) Normalized drain current change *S* obtained with 4 different configurations: response to NF-Y with the CCAAT-containing dsDNA probe immobilized on the gate (red, labelled as Probe); control experiment based on the response to NF-Y with a mutated probe immobilized on the gate (green, labelled as M-Probe), control experiment based on the response to NF-Y in the absence of the oligonucleotide probe on the gate, i.e. with only a MUA/MCH SAM on the gate (blue, labelled as C-SAM) and control experiment based on the response to a non-relevant protein (IgG1 antibody) with the CCAAT-containing dsDNA probe immobilized on the gate (yellow, labelled as C-Target). The signal is reported with standard error of the mean error bars obtained with 6 datasets for Probe and M-Probe, and 3 datasets for C-SAM and C-Target. d) Loadings (blue axis and vectors) and scores (black axis) plot obtained from the PCA analysis. The data points areas are coloured according to the respective type of sample: probe/target (red), mutated-probe/target (green), the control experiment with only SAM on the gate (blue) and the control experiment with a different target (yellow).

be used to quantify the response of the biosensor to the analyte binding. The variation of I_{DS}, transconductance (g_m) or threshold voltage (V_{th}) as function of analyte concentration can be exploited to build the signal of the sensor. Here, we calculate the signal based on the I_{DS} variations, as $S = \Delta I/I_0$, where ΔI is the I_{DS} in presence of NF-Y at V_{GS} = –0.6 V minus I0, which is the I_{DS} without the target analyte at the same V_{GS}.

As reported in Fig. 5b, the signal shows a non-linear increase with increasing NF-Y concentration, reaching saturation around 10 nM. The calibration curves of biosensors based on binding interactions are often modelled with a Langmuir binding model to obtain a binding isotherm that relates the signal magnitude with the analyte concentration.[45–48] In this case, the Langmuir model does not provide a good fit of the experimental data. As an alternative, we fitted the dose curve with the uniform Langmuir absorption model, defined as follow:

$$S = \frac{S_{max}}{2A} ln\left(\frac{1+K_{avg}[NFY-L]e^{A}}{1+K_{avg}[NFY-L]e^{-A}}\right) (1)$$

where S_{max} is the plateau reached at 10 nM, K_{avg} is the average binding constant of a probe layer with uniform distribution of binding energies U in the range between U_{max} and U_{min}.,[48,49] and

$$A = \frac{(U_{max}-U_{min})}{2k_BT} (2)$$

Equation 1 recovers the Langmuir isotherm in a system where all binding sites are homogeneous, meaning that the binding energies are monodispersed, and the parameter A tends to 0:

$$S = S_{max}\frac{K_{avg}[NFY-L]}{1+K_{avg}[NFY-L]} (3)$$

From the best fit of the data with eq. 1, using the parameters S_{max}, A, and K_{avg}, we extract the values S_{max} = 1.2, the dissociation constant $1/K_{avg}=1 \times 10^{-11}$, which is in line with the values reported in literature determined by in solution assays,[50,51] and the value U_{max}-U_{min} =26.8 kJ/mol from the best fit parameter A assuming room temperature. This broad energy dispersion (about 10 times the thermal energy) could be ascribed to the mobility of immobilized DNA strands and the local structural variability of the SAM.

We then performed a set of control experiments to assess the selectivity of the biosensor, by modifying either the probe on the gate or the target species in solution and comparing the response S with respect to the values obtained with the CCAAT-containing dsDNA in the presence of NF-Y.

The first set of controls, labelled as “M-Probe” in Fig. 5c, was performed by immobilizing on the gate a dsDNA mutated in the consensus sequence (see sequence in materials and methods section) and by exposing the gate to NF-Y. As shown in Fig. 5c, the signal S of M-probe (green bars) is always lower than the one obtained with the wild-type Probe (red bars) but still significant. To verify if this behavior was due to non-specific absorption of NF-Y on the SAM or a weak interaction between NF-Y and the mutated probe, we performed control experiments where no dsDNA was immobilized on the gate, but just the SAM treated with EDC/NHS and TRIS (labelled “C-SAM”). The signal S of the C-SAM (blue bars) shows very small values, insensitive to concentration, suggesting a negligible absorption of NF-Y on the SAM surface. As a last control, we incubated the gate functionalized with the probe in a solution containing an IgG1 antibody (MW = 150 KDa), to evaluate the non-specific absorption of proteins on the gate. As shown in Fig. 5c, the S response (yellow bars) is always much smaller than the Probe (red bars), but not negligible, indicating some non-specific binding occurs. In brief, the set of control experiments underlines the high degree of selectivity of the sensor, together with a small amount of non-specific absorption.

These data demonstrate that the specific (NF-Y), else the non-specific, binding events (control experiments) produce profoundly different effects on the transistor current. Therefore, we also evaluated the signal of the transconductance (S_{gm}) and the shift of the threshold voltage (ΔV_{th}) to quantitatively discriminate the signal from NF-Y experiments from that of the controls, by means of a principal component analysis (PCA).[52-54] PCA is widely used for multi-variate data visualization and dimensionality reduction. PCA transforms a dataset dependent on potentially correlated variables into a new set of uncorrelated variables, called principal components (PCs). Here, the signal of the current, signal of transconductance and difference of threshold voltage were used independent variables for the calculation of the PCs. The results are reported in Fig. 5d: the loading plot (blue axis) show that S and S_{gm} are highly correlated, while the contribution of ΔV_{th} to the PC1 (86.65% of the variance) and PC2 (11.53% of the variance) is almost orthogonal to the contribution of the other two. In the scores plot (Fig. 5d, black axis) each point represents the average of at least three different samples at a particular experimental condition. The combination of PC1 and PC2 can effectively distinguish between samples containing NF-Y with respect to the control samples, except for the standard at 1 pM NF-Y, whose score place is very close to the region of the ‘C-SAM’ samples. Furthermore, we note that the scores of the ‘Probe’ samples set is also correlated with the concentration of NF-Y, as should be expected given that both S and ΔV_{th} are

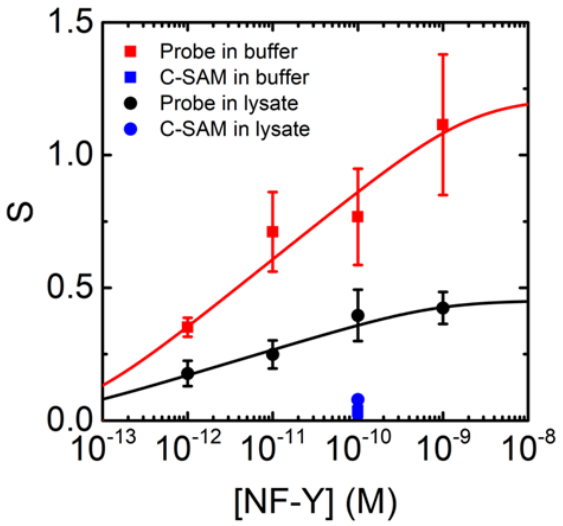

Fig. 6 NF-Y detection in cell lysate. Signal of the current upon detection of NF-Y in 1:10 lysate with the probe (black, dots) or with only the SAM on the gate (blue dot), compared with the experiments performed in PBS buffer with the probe (red squares) and C-SAM (blue square). Data in lysate obtained with 3 datasets, reported with standard error of the mean. The data in red are the same shown in Fig. 5b, without the10 nM point.

correlated with the analyte concentration. The use of a PCA analysis to organize and cluster the response obtained with the EGOT biosensor provides a clear view of the multiparametric nature of the response and the correlation between parameters, allowing the discrimination between selected targets and control experiments.

To assess the response of the device in a more complex matrix, as in biopsies from patients, we spiked diluted HEK293 cell lysate (1:10 in 1X PBS) with a standard solution of recombinant NF-Y. As shown in Fig. 6, we observe that the device is still able to detect NF-Y in the lysate, although the signal magnitude is ~30% than the one obtained in PBS. More specifically, the signal S shows an increase in the 1 pM–100 pM range, concentration after which the values saturate. The control, made with only the SAM formed on the gate but without the dsDNA probe ('C-SAM' experimental condition), shows that 100 pM NF-Y in lysate generates a signal that is ~20% of the one obtained with the same concentration of TF with the probe on the gate. These preliminary data demonstrate the possibility to detect NF-Y also in cell lysate, although further improvement is needed to achieve precise quantification of the target.

Conclusions

We presented the first EGOT biosensor for transcription factors, based on the detection of the heterotrimeric TF NF-Y by its consensus DNA sequence immobilized on a gold electrode, amplified by the TIPS-pentacene channel. Thanks to a set of control experiments, we can safely ascribe the signal of the device to the binding of NF-Y to the probe DNA on the gate. The biosensor can detect the TF in concentrations between 1pM and 10 nM in buffer, showing a multiparametric response, that can be evaluated in terms of current change. We observed that DNA probes mutated in the consensus region show a non-zero response, underlining possible weak interactions between NF-Y and the lateral sequences of the DNA probe. We estimated a LOD of 10 fM, which is in the order of magnitude of the lowest LOD reported in literature for a TF (NF-κB).[55] To move towards the use of the biosensor with patients' samples, we demonstrated the detection of NF-Y in cell lysate, mimicking the analysis of cell lysates from biopsies. The response of the biosensor in lysate is lower compared to the one recorded in buffer but is still clearly distinguishable from the control experiments. Exon 3 splicing occurs within the mRNA region encoding the NF-YA transactivation-N-terminal domain and should not alter the ability of NF-YA short and long isoforms to interact with the NF-YB/NF-YC subunits and with DNA targets, with this domain being at the C-terminus. Despite this, recent data highlighted that NF-YAs-composed and NF-YAl-composed NF-Y complexes differently bind and transcriptionally regulate target genes[9]. The ability of NF-YAl to induce a pro-metastatic signature in cancer cells and the possibility to use NF-YAl levels as a prognostic molecular marker in cancer patients raises the need to quantify its expression although an isoform-specific antibody is lacking. The EGOT biosensor for NF-Y is the first TF biosensor based on EGOTs and represents a starting point for the realization of point-of-care devices for the NF-YA isoforms detection and discrimination. We believe that this work contributes to removing some bottlenecks that are still relevant in the field of EGOT biosensors and to introducing promising future applications. First, by implementing a multivariate analysis and a set of control experiments, we can safely attribute the change of a single transistor figure of merit (fom) to a selective biorecognition event or to other processes like non-specific absorption effects. Furthermore, the multivariate analysis allows us to consider the complexity of the EGOT response, showing that the combination of different foms could lead to a better monitoring of the biorecognition process. Second, we show the first EGOT able to detect a transcription factor, which opens interesting perspectives not only in the development of biosensors but also in the use of this platform for further studies about the interactions between TFs and DNA sequences. Third, the present study strengthens the effectiveness of EGOT biosensors in a complex matrix, like the one represented by cell lysates, suggesting the possibility to monitor the presence of target biomarkers in biopsies.

Experimental

Chemicals

1X PBS, potassium ferricyanide, potassium chloride, hexane, toluene, MUA, MCH and TRIS were purchased from Sigma-Aldrich. TIPS-pentacene was purchased from Ossila.

DNA sequences

The oligonucleotides were purchased from IDT and diluted in 1X PBS at pH 8.

Probe: 5'-/AmMC6/TTC TGA GCC AAT CAC CGA GCT CGA T-3'

Target: 5'-ATC GAG CTC GGT GAT TGG CTC AGA A-3'

Mutated-Probe: 5'-/AmMC6/TTC TGA GTT GGC CAC CGA GCT CGA T-3'

Mutated-Target: 5'-ATC GAG CTC GGT GGC CAA CTC AGA A-3'

Protein production and purification

Recombinant plasmids for bacterial expression of Trx-tagged-NF-YA long isoform and 6His-tagged NF-YC (37 kDa isoform) were previously described.56 The plasmid encoding NF-YB N-terminal portion (aa 1-141), including the HFD, was obtained by subcloning the mouse NF-YB HFD coding sequence57 into the pnEATH vector backbone, and subsequently replacing the NF-YB 5' end with the NdeI-MunI fragment derived from pET3-NF-YB,58 obtaining an un-tagged recombinant protein construct. The soluble NF-YB/NF-YC dimer was produced by co-expressing the subunits constructs in E. coli BL21(DE3). Recombinant NF-YA and NF-YB/NF-YC dimer were purified by Ion-Metal Affinity Chromatography (IMAC), using His-Select Nickel affinity resin (Sigma Aldrich), as described,56 by exploiting the 6His affinity tag on the NF-YA or NF-YC subunits, respectively. The NF-YB/NF-YC dimer was further purified by Size Exclusion Chromatography in Buffer B (10 mM Tris-HCl pH 8.0, 400 mM NaCl, 10% glycerol, 2 mM DTT).

NF-Y complex in vitro reconstitution, immunoprecipitation, and immunoblotting

NF-YAl and NF-YB/NF-YC recombinant proteins were incubated to form the NF-Y heterotrimer in 100 mM salt solution for 2h in ice. 20 µl of Protein G-Agarose were incubated in 100 µl of NDB100 buffer (100 mM KCl, 20 mM HEPES pH 7.9, 0.1% NP-40, 0.5 mM EDTA, 1 mM phenylmethylsulfonyl fluoride) to which 7 µg of anti-NF-YB (GeneSpin) or 3 µg of anti-NF-YA (Diagenode) antibodies had been bound for 2h at 4°C with rotation. The NF-Y trimer (500 ng) was added to the G-Protein/Antibody complex and incubated overnight with rotation at 4°C. Unbound material was recovered after centrifugation and the G-protein was washed twice with NDB100 buffer. SDS sample buffer (25 mM TrisHCl pH 6.8, 1.5 mM EDTA, 20% glycerol, 2% SDS, 5% β-mercaptoethanol, 0.0025% Bromophenol blue) was added and the samples were boiled at 95°C for 5 min and loaded to SDS gel. To confirm that interaction occurs between the three subunits, we performed an immunoprecipitation assay with anti-NF-YB or anti-NF-YA antibodies followed by western blot analysis of the three subunits.

For immunoblotting, equivalent amounts of cellular extracts were resolved by SDS-PAGE, electrotransferred to PVDF membrane (GE Healthcare) and immunoblotted with the following primary antibodies diluted 1:1000 in TBS 1X- BSA 1 µg/µl: anti-NF-YA (Thermo Fisher Scientific), anti-NF-YB (GeneSpin), anti-NF-YC (GeneSpin). After washes with TBS 1X membranes were incubated with secondary antibody HRP conjugated goat anti-rabbit (ThermoFisher Scientific) diluted 1:5000. Membranes were blotted and scanned with Amersham Imager AI680 RGB (GE Healthcare), using chemiluminescent detection reagents Westar ηC and Supernova HRP substrates (Cyanagen).

Gate functionalization

The Gate was functionalized with the following protocol: i) The Au electrodes were incubated overnight in 1:3 MUA/MCH in ethanol; ii) incubation for 30 minutes in EDC and NHS (200 mM and 50 mM in MES respectively; iii) binding of a 10 µM 26 base-pairs oligonucleotide, containing a C-6 space, the CCAAT box and a terminal amine, to the carboxylic groups of MUA for 1h; iii) 1 µM complementary oligonucleotide hybridization, iv) incubation in 10 mM Tris, for 30 minutes, to block unreacted intermediates. The functionalized gate was incubated in NF-Y solutions at various concentrations for 20 minutes and then rinsed with the buffer before measurement.

EGOT fabrication

Mircux gold IDE electrodes (L=10 µm) on glass were cleaned by three steps of 15 minutes of ultrasonication in Hellmanex 1%, distilled water and ethanol, rinsing with the same solution and drying with N_2 after each step.

A drop of 1 µL Tips-pentacene 2% in toluene/hexane 80:20 was casted on the interdigitated electrodes and then the device was cured on heating plate at 60°C for 30 minutes.

As many as 25-30 devices were processed. The key performance indicators of the transistor, their reproducibility and stability are reported in Table S1 and Figure S1 in Supplementary Information.

Electrical characterization

The transfer curves were measured with an Agilent B2902A Source Measure Unit (SMU), by fixing the V_{DS} at −0.2 V and sweeping the V_{GS} between 0 V and -0.7 V. The electrolyte was confined in a PDMS pool and consisted of 40 µL of 1X PBS at pH 7.4.

Limit of detection

The LOD was defined as the concentration of NF-YA that corresponds to a signal of $S_0+3\sigma$, where S_0 is the signal of the signal of the blank at V_{GS} =-0.5 V, and σ is the standard deviation of blank transfer curves.[59]

Electrochemical characterization

The electrochemical measurements were performed in a three electrodes configuration with a CHInstruments potentiostat 760c. The gold gate was connected as the working electrode, an Ag/AgCl electrode as reference electrode and a platinum wire as counter electrode. The three electrodes were immersed in a glass electrochemical cell, filled with the 5 mm $K_3Fe(CN)_6$, 0.1 M KCl. The potential was set to 0.27 V, with an amplitude of 10 mV and in the range of frequencies from 0.1 Hz to 100 kHz. The EIS fitting was performed with EIS Spectrum Analyzer software. [60] We fitted the Nyquist plots with a Randles circuit, where we replaced the capacitor with a constant phase element to reproduce the complexity of the gate functionalization.

Principal Component Analysis (PCA)

For the PCA, the samples signals calculated with I_{DS} and g_m and the ΔV_{th}, are the input dataset. $S(I_{DS})$, $S(g_m)$ and ΔV_{th} are the variables and the signals or V_{th} shifts recorded at increasing analyte/control concentration are the observations. The variables of the input matrix are pre-processed with the mean-centering method, to express data as deviation from the mean value. PCA is performed via singular value decomposition algorithm on the input matrix. The dimensionality of the final PCA model was set at two principal components (PC1 and PC2), explaining 98.18% of the input dataset variance. Results of the PCA were represented by plotting loading and scores plot of PC1 vs PC2.

Conflicts of interest

There are no conflicts to declare.

Acknowledgements

This paper is dedicated to Prof. Gilles Horowitz, a friend and a scientist that contributed important insights in organic field effect transistors. M.S. was supported by Fondazione Umberto Veronesi. The publication has been realized with the co-financing of European Union - FSE-REACT-EU, PON research and Innovation 2014-2020 DM1062/2021.

References

1 J. H. Bushweller, Nat Rev Cancer, 2019, 19, 611–624.
2 A. Gurtner, I. Manni and G. Piaggio, Biochim Biophys Acta Gene Regul Mech, **2017**, 1860, 604–616.
3 S. N. Maity, *Biochim Biophys Acta*, **2017**, 1860, 598–603.
4 G. Rigillo, V. Basile, S. Belluti, M. Ronzio, E. Sauta, A. Ciarrocchi, L. Latella, M. Saclier, S. Molinari, A. Vallarola, G. Messina, R. Mantovani, D. Dolfini and C. Imbriano, *Nat Commun*, **2021**, 12, 1–17.
5 P. Benatti, D. Dolfini, A. Vigan, M. Ravo, A. Weisz and C. Imbriano, *Nucleic Acids Res*, **2011**, 39, 5356–5368.
6 P. Benatti, M. L. Chiaramonte, M. Lorenzo, J. A. Hartley, D. Hochhauser, N. Gnesutta, R. Mantovani, C. Imbriano and D. Dolfini, *Oncotarget*, **2015**, 7, 1633–1650.
7 S. Belluti, V. Semeghini, G. Rigillo, M. Ronzio, D. Benati, F. Torricelli, L. Reggiani Bonetti, G. Carnevale, G. Grisendi, A. Ciarrocchi, M. Dominici, A. Recchia, D. Dolfini and C. Imbriano, *Journal of Experimental and Clinical Cancer Research*, **2021**, 40, 1–23.
8 D. Dolfini, V. Andrioletti and R. Mantovani, Sci Rep, **2019**, 9, 1–12.
9 G. Rigillo, S. Belluti, V. Campani, G. Ragazzini, M. Ronzio, G. Miserocchi, B. Bighi, L. Cuoghi, V. Mularoni, V. Zappavigna, D. Dolfini, L. Mercatali, A. Alessandrini and C. Imbriano, *Cancer Lett*, **2023**, 567, 216262.
10 V. Nardone, A. Chaves-Sanjuan, M. Lapi, C. Airoldi, A. Saponaro, S. Pasqualato, D. Dolfini, C. Camilloni, A. Bernardini, N. Gnesutta, R. Mantovani and M. Nardini, *Cells*, **2020**, 9, 1–21.
11 X. Fang, H. Han, G. Stamatoyannopoulos and Q. Li, Journal of Biological Chemistry, **2004**, 279, 5444–5449.
12 S. Belluti, G. Rigillo and C. Imbriano, *Cells*, **2020**, 9, 760.
13 V. Basile, F. Baruffaldi, D. Dolfini, S. Belluti, P. Benatti, L. Ricci, V. Artusi, E. Tagliafico, R. Mantovani, S. Molinari and C. Imbriano, *Biochim Biophys Acta*, **2016**, 1859, 627–638.
14 D. Dolfini, M. Minuzzo, G. Pavesi and R. Mantovani, Stem *Cells*, **2012**, 30, 2450–2459.
15 E. Bezzecchi, M. Ronzio, D. Dolfini and R. Mantovani, *Genes*, **2019**, 10, 937.
16 E. Bezzecchi, M. Ronzio, V. Semeghini, V. Andrioletti, R. Mantovani and D. Dolfini, *Genes*, **2020** , 11, 198.
17 M. Londero, A. Gallo, C. Cattaneo, A. Ghilardi, M. Ronzio, L. Del Giacco, R. Mantovani and D. Dolfini, *Cell Death Dis*, **2023**, 14, 65.
18 L. Sha, X. Zhang and G. Wang, *Biosens Bioelectron*, **2016**, 82, 85–92.
19 Z. Fan, J. Wang, N. Hao, Y. Li, Y. Yin, Z. Wang, Y. Ding, J. Zhao, K. Zhang and W. Huang, *Chemical Communications*, **2019**, 55, 11892–11895.
20 E. A. Nalefski, E. Nebelitsky, J. A. Lloyd and S. R. Gullans, *Biochemistry*, **2006**, 45, 13794–13806.
21 F. Torricelli, D. Z. Adrahtas, Z. Bao, M. Berggren, F. Biscarini, A. Bonfiglio, C. A. Bortolotti, C. D. Frisbie, E. Macchia, G. G. Malliaras, I. McCulloch, M. Moser, T.Q. Nguyen, R. M. Owens, A. Salleo, A. Spanu and L. Torsi, *Nat. Rev. Methods Primers*, **2021** , 1, 66.
22 X. Jiang, C. Shi, Z. Wang, L. Huang and L. Chi, *Adv Mater*, **2023**, 2308952, 1–39.
23 B. Piro, D. Wang, D. Benaoudia, A. Tibaldi, G. Anquetin, V. Noël, S. Reisberg, G. Mattana and B. Jackson, *Biosens Bioelectron*, **2017**, 92, 215–220.
24 R. Massey, S. Bebe and R. Prakash, *IEEE Sens Lett*, **2020**, 4, 7.
25 L. Kergoat, B. Piro, M. Berggren, M. Pham and A. Yassar, *Org Electron*, **2012**, 13, 1–6.
26 J. Rivnay, S. Inal, A. Salleo, R. M. Owens, M. Berggren and G. G. Malliaras, *Nat Rev Mater*, **2018** ,3.
27 C. Diacci, T. Abedi, J. Lee, E. O. Gabrielsson, M. Berggren, D. T. Simon, T. Niittylä and E. Stavrinidou, *iScience*, **2020**, 101966.
28 M. Sensi, M. Berto, S. Gentile, M. Pinti, A. Conti, G. Pellacani, C. Salvarani, A. Cossarizza, C. A. Bortolotti and F. Biscarini, *Chem Commun*, **2021**, 57, 367–370.
29 K. Solodka, M. Berto, D. Ferraro, C. Menozzi, M. Borsari, C. A. Bortolotti, F. Biscarini and M. Pinti, *Adv Mater Interfaces*, **2022**, 9, 2102341.
30 M. Berto, M. Di Giosia, M. Giordani, M. Sensi, F. Valle, A. Alessandrini, C. Menozzi, A. Cantelli, G. C. Gazzadi, F. Zerbetto, M. Calvaresi, F. Biscarini and C. A. Bortolotti, *Adv Electron Mater*, **2021**, 7, 200114.
31 E. Macchia, K. Manoli, B. Holzer, C. Di Franco, M. Ghittorelli, F. Torricelli, D. Alberga, G. F. Mangiatordi, G. Palazzo, G. Scamarcio and L. Torsi, *Nat Commun*, **2018**, 9, 3223.
32 R. K. Mendes, R. S. Freire, C. P. Fonseca, S. Neves and L. T. Kubota, *J Braz Chem Soc*, **2004**, 15, 849–855.
33 F. S. Damos, R. C. S. Luz and L. T. Kubota, *Langmuir*, **2005**, 21, 602–609.
34 T. C. Tsai, C. W. Liu, Y. C. Wu, N. A. P. Ondevilla, M. Osawa and H. C. Chang, *Colloids Surf B Biointerfaces*, **2019**, 175, 300–305.
35 M. Sensi, R. F. de Oliveira, M. Berto, M. Palmieri, E. Ruini, P. A. Livio, A. Conti, M. Pinti, C. Salvarani, A. Cossarizza, J. M. Cabot, J. Ricart, S. Casalini, M. B. González-García, P. Fanjul-Bolado, C. A. Bortolotti, P. Samorì and F. Biscarini, *Adv Mater*, **2023**, 35, 1–9.
36 H. Gui, B. Wei and J. Wang, *Mater Sci Semicond Process*, **2015**, 30, 250–254.
37 S. Pan and L. Rothberg, *Langmuir*, **2005**, 21, 1022–1027.
38 M. Gebala and W. Schuhmann, *ChemPhysChem*, **2010**, 11, 2887–2895.
39 J. Kafka, O. Pänke, B. Abendroth and F. Lisdat, *Electrochim Acta*, **2008**, 53, 7467–7474.
40 Y. Zhang, X. Geng, J. Ai, Q. Gao, H. Qi and C. Zhang, *Sens Actuators B Chem*, **2015**, 221, 1535–1541.
41 W. Bi, L. Wu, F. Coustry, B. de Crombrugghe, and S. N. Maity, J Biol Chem, **1997**, 272(42), 26562–26572.
42 M. D. Biggin, *Dev Cell*, **2011**, 21, 611–626.
43 M. S. Thomas, S. P. White, K. D. Dorfman and C. D. Frisbie, *J Phys Chem Lett*, **2018**, 9, 1335–1339.
44 G. Palazzo, D. De Tullio, M. Magliulo, A. Mallardi, F. Intranuovo, M. Y. Mulla, P. Favia, I. Vikholm-Lundin and L. Torsi, *Adv Mater*, **2015**, 27, 911–916.
45 P. A. Manco Urbina, M. Berto, P. Greco, M. Sensi, S. Borghi, M. Borsari, C. A. Bortolotti and F. Biscarini, *J Mater Chem C*, **2021**, 9, 10965–10974.
46 H. Swenson and N. P. Stadie, *Langmuir*, **2019** , 35, 5409-5426.
47 L. Vanjur, T. Carzaniga, L. Casiraghi, M. Chiari, G. Zanchetta and M. Buscaglia, *Biophys J*, **2020**, 119, 989–1001.
48 R. A. Latour, *J Biomed Mater Res A*, **2015**, 103, 949–958.
49 A. Paradisi, M. Berto, M. Di Giosia, S. Mazzali, M. Borsari, T. D. Marforio, F. Zerbetto, M. Calvaresi, A. Orieshyna, N. Amdursky, C. A. Bortolotti and F. Biscarini, *Chem Eur J,* **2023**, 29, e202301704.
50 M. Nardini, N. Gnesutta, G. Donati, R. Gatta, C. Forni, A. Fossati, C. Vonrhein, D. Moras, C. Romier, M. Bolognesi and R. Mantovani, *Cell*, **2013**, 152, 132–143.
51 D. Dolfini, R. Gatta and R. Mantovani, *Crit Rev Biochem Mol Biol*, **2012**, 47, 29–49.
52 E. Martynko and D. Kirsanov, *Biosensors*, **2020** ,10 ,100.
53 E. Genco, F. Modena, L. Sarcina, K. Björkström, C. Brunetti, M. Caironi, M. Caputo, V. M. Demartis, C. Di Franco, G. Frusconi, L. Haeberle, P. Larizza, M. T. Mancini, R. Österbacka, W. Reeves, G. Scamarcio, C. Scandurra, M. Wheeler, E. Cantatore, I. Esposito, E. Macchia, F. Torricelli, F. A. Viola, L. Torsi, *Adv Mater*, **2023**, 35, 2304102.

54 E. Macchia, F. Torricelli, M. Caputo, L. Sarcina, C. Scandurra, P. Bollella, M. Catacchio, M. Piscitelli, C. Di Franco, G. Scamarcio, L. Torsi, *Adv Mater*, **2023**, 2309705.
55 B. Li, S. Xie, A. Xia, T. Suo, H. Huang, X. Zhang, Y. Chen, and X. Zhou, *TrAC - Trends in Analytical Chemistry*, **2020**, 132, 116039.
56 A. Bernardini, M. Lorenzo, A. Chaves-Sanjuan, P. Swuec, M. Pigni, D. Saad, P. V. Konarev, M. A. Graewert, E. Valentini, D. I. Svergun, M. Nardini, R. Mantovani and N. Gnesutta, *Int J Biol Macromol*, **2021**, 193, 401–413.
57 M. Nardini, N. Gnesutta, G. Donati, R. Gatta, C. Forni, A. Fossati, C. Vonrhein, D. Moras, C. Romier, M. Bolognesi and R. Mantovani, *Cell*, **2013**, 152, 132–143.
58 R. Mantovani, U. Pessara, F. Tronche, X.-Y. Li, A.-M. Knapp, J.-L. Pasquali, C. Benoist and D. Mathis, *EMBO J*, **1992**, 1, 3315–3322.
59 A. D. McNaught, A. Wilkinson, IUPAC Compendium of Chemical Terminology, 2nd Ed. (the “Gold Book”), *Blackwell Scientific Publications*, Oxford,**1997**, 839.
60 A. S. Bondarenko, G. A. Ragoisha, Progress in Chemometrics Research, *Nova Science Publishers*, New York, **2005**, 89–102.